Mon. Not. R. Astron. Soc. **425,** 1967–1979 (2012) doi:10.1111/j.1365-2966.2012.21518.x

The halo shape and evolution of polar disc galaxies

O. N. Snaith,[1,2,3]★ B. K. Gibson,[1,4,5] C. B. Brook,[1,6] A. Knebe,[6] R. J. Thacker,[4] T. R. Quinn,[7] F. Governato[7] and P. B. Tissera[2]

[1]*Jeremiah Horrocks Institute, University of Central Lancashire, Preston PR1 2HE*
[2]*Instituto de Astronomía y Física del Espacio, Conicet-UBA, CC67, Suc. 28, 1428 Ciudad de Buenos Aires, Argentina*
[3]*GEPI, Observatoire de Paris, CNRS, Univ. Paris Diderot, 5 Place Jules Janssen, F-92195 Meudon, France*
[4]*Department of Astronomy & Physics, Saint Mary's University, Halifax, Nova Scotia B3H 3C3, Canada*
[5]*Monash Centre for Astrophysics, School of Mathematical Sciences, Monash University, Clayton, VIC 3800, Australia*
[6]*Grupo de Astrofiísica, Depatamento de Fisica Teorica, Universidad Autónoma de Madrid, Cantoblanco E-280049, Spain*
[7]*Department of Astronomy, University of Washington, Seattle, WA 98195, USA*

Accepted 2012 June 12. Received 2012 June 11; in original form 2011 November 23

ABSTRACT

We examine the properties and evolution of a simulated polar disc galaxy. This galaxy is composed of two orthogonal discs, one of which contains old stars (old stellar disc) and the other both younger stars and cold gas (polar disc). By exploring the shape of the inner region of the dark matter halo, we are able to confirm that the halo shape is an oblate ellipsoid flattened in the direction of the polar disc. We also note that there is a twist in the shape profile, where the innermost 3 kpc of the halo flattens in the direction perpendicular to the old disc and then aligns with the polar disc out until the virial radius. This result is then compared to the halo shape inferred from the circular velocities of the two discs. We also use the temporal information of the simulation to track the system's evolution and identify the processes which give rise to this unusual galaxy type. We confirm the proposal that the polar disc galaxy is the result of the last major merger, where the angular moment of the interaction is orthogonal to the angle of the infalling gas. This merger is followed by the resumption of coherent gas infall. We emphasize that the disc is rapidly restored after the major merger and that after this event the galaxy begins to tilt. A significant proportion of the infalling gas comes from filaments. This infalling gas from the filament gives the gas its angular momentum, and, in the case of the polar disc galaxy, the direction of the gas filament does not change before or after the last major merger.

Key words: galaxies: evolution – galaxies: formation – galaxies: haloes – galaxies: interactions – galaxies: structure.

1 INTRODUCTION

Classical disc galaxies consist of flattened distributions of stars, gas and dust, corotating with the angular momentum vectors more or less aligned;[1] polar disc galaxies[2] are significantly more rare, possessing two orthogonal discs. An original survey of galaxies consisting of orthogonal structures of stars was carried out by Whitmore et al. (1990), who identified a sample of polar *ring* galaxies. The 'primary' discs in such systems are typically classified as lenticulars (S0), or ellipticals, with a second, younger, structure aligned with the angular momentum axis of the primary disc. Fewer than 1 per cent of S0 galaxies contain a polar structure.

Subsequent studies of NGC 4650A revealed a subclass of structures where the orthogonal distribution of stars was not a *ring* but a second fully formed continuous *disc* structure (Gallagher et al. 2002; Iodice et al. 2002; Swaters & Rubin 2003; Macciò, Moore & Stadel 2006; Brook et al. 2008). Systematic studies suggest that their stellar populations, light distribution and gas-phase characteristics are not dissimilar from those of classical discs – e.g. exponential light profiles (Schweizer, Whitmore & Rubin 1983) and H I mass-to-optical luminosities typical of mass-to-*B*-band luminosity typical of late-type spirals (Arnaboldi et al. 1997; Huchtmeier 1997; Sparke & Cox 2000; Cox, Sparke & van Moorsel 2006).

Thus, there exist *polar ring* galaxies as well as *polar disc* galaxies. We will discuss the latter type in this paper. One of the important uses of polar disc galaxies is a direct result of having orthogonal discs at the bottom of a halo potential well. One stellar disc

★E-mail: onsnaith@hotmail.co.uk
[1] In the presence of warps, though, there may be some misalignment driven by external torques (Roškar et al. 2010).
[2] Originally called 'multispin galaxies' by Rubin (1994).

historically allowed astronomers to calculate the existence of dark matter haloes (see Begeman, Broeils & Sanders 1991, for a detailed discussion). Iodice et al. (2003) note that the existence of two orthogonal discs means that the shape of the inner region of the halo can be recovered from observations.

There are several theories proposed to explain the origin of polar ring and polar disc galaxies.

(i) *Mergers*. As envisioned by Bekki (1997, 1998) and Bournaud & Combes (2003), polar rings can eventuate for very specific collision configurations where the collision is 'head-on' and the initial angular momentum low.

(ii) *Tidal accretion*. Proposed by Schweizer et al. (1983) and simulated by Reshetnikov & Sotnikova (1997), this scenario involves the capture of a gas-rich secondary by the (future) polar disc host halo. The interaction-induced polar ring is formed more readily than in the aforementioned merger-induced scenario (Bournaud & Combes 2003; Combes et al. 2006).

(iii) *Infall from filaments*. If gas falls into a galaxy along cosmic filaments that are inclined to the stellar disc, a polar disc may form (Macciò et al. 2006; Brook et al. 2008). Combes et al. (2006) and Bournaud & Combes (2003) suggest that such cosmological infall is a viable alternative to tidal accretion for the NGC 4650A system (e.g. Iodice et al. 2006; Spavone et al. 2010, 2011).

(iv) *Resonance*. This approach assumes that the polar disc is formed via resonant coupling to a triaxial halo potential (Tremaine & Yu 2000). In this picture, a disc is taken to lie in the plane of symmetry of the triaxial halo and the halo tumbles with respect to the disc. As the tumbling slows, the stars in the disc can get trapped in resonance with the halo. A stellar orbit inclined to the disc precesses at a slow retrograde rate and the star can be pushed into a polar orbit. This method has been invoked to best explain equal-mass stellar disc systems.

A seminal review of the field is provided by Combes et al. (2006), to which all interested readers should refer for a rich survey of the field. The filamentary infall scenario (iii, above) of Macciò et al. (2006) has gathered momentum over the past few years as being the favoured origin of polar disc systems. This can be traced, in part, to the fact that the alternatives do not account fully for the range of observations – in particular, those which show that the polar disc is often of high mass, possesses extended and continuous structure, and lacks obvious evidence of starbursts that might be associated with polar structure formation. A polar disc/ring galaxy can be formed by scenario (i) when the relative initial velocities are low (e.g. Bournaud & Combes 2003) and by (ii) in loose groups of galaxies such as UGC 9796 (Spavone et al. 2011). Polar disc/ring galaxies are found in low-density environments as the polar structure is destroyed by mergers (Macciò et al. 2006). This suggests that each type of formation may exist in the Universe.

Closely related to Macciò et al. (2006) scenario (iii, above), Brook et al. (2008) suggest that the polar disc forms as a result of the last major merger changing the angular momentum of the stars and gas of the stellar disc, and then subsequent gas continues to fall in along the old trajectory and builds up the polar disc.[3] The basic observable characteristics of their simulated polar disc system were presented, including star formation rates (SFRs), circular velocity profiles and structural parameters of the discs, along with the aforementioned putative origin scenario. The exact mechanism by which the dark halo aligns to the orthogonal discs and how the new infalling gas becomes misaligned to the orthogonal discs was *not* studied by Brook et al. (2008).

In what follows, we rectify this by examining the underlying physics governing the misalignment of the discs in the Brook et al. (2008) simulation, tracing its temporal evolution and association with large-scale structure, in order to put their origin scenario to the test, quantitatively. The simulation and its basic properties are reviewed in Sections 2 and 3, while the time evolution of the host halo's shape is detailed in Section 4. The metallicity and age gradients of the discs are then confronted with recent observational work (Section 5), while the time evolution of the dark halo, gas and stellar angular momenta is derived in Section 6. Our conclusions and suggestions for future directions are made in Section 7.

2 CODE

The polar disc system under examination here was realized with the gravitational N-body+smoothed particle hydrodynamics (SPH) code GASOLINE (Wadsley, Stadel & Quinn 2004). Gravitational forces are computed using a Barnes & Hut (1986) tree-based algorithm; the code is spatially and temporally adaptive and employs periodic boundary conditions. SPH is used to discretize the astrophysical gas and accounts for radiative cooling, ionization and excitation of the gas. The ultraviolet background radiation field is included, after Haardt & Madau (1996). The internal energy of the gas is calculated to conserve energy better than entropy, and shocks are accounted for via artificial viscosity.

The star formation recipe employed within GASOLINE is detailed by Stinson et al. (2006) and includes (i) a Kroupa (2001) initial mass function, (ii) the effects of both Type Ia and Type II supernovae (neglecting the instantaneous recycling approximation) and (iii) a blast-wave feedback scheme with which to couple supernova energy to the surrounding interstellar medium.

For this simulation, first introduced by Brook et al. (2008), volume renormalization was employed to ensure high spatial and force resolution in the area of interest while self-consistently tracking the gravitational torques imparted by large-scale cosmological structure. The cosmological framework was a concordant Λ cold dark matter, with $\Omega_0 = 0.3$, $\Omega_\Lambda = 0.7$, $\sigma_8 = 0.81$, $h = 0.7$, where Ω_0 is the matter density, Ω_Λ is the fraction of the energy density of the Universe due to the cosmological constant, σ_8 is the rms density fluctuation in 8 Mpc subsamples and h the Hubble constant. The initial power spectrum was calculated using CMBFAST (Seljak & Zaldarriaga 1996; Zaldarriaga, Seljak & Bertschinger 1998).

An initial, coarse, dark matter only simulation was run to redshift $z = 0$ in a $28.5\,h^{-1}$ Mpc box; this is large enough to provide realistic tidal torques with sufficient resolution for halo identification. A host halo was selected using AHF (Gill, Knebe & Gibson 2004; Knollmann & Knebe 2009), and the particles therein traced back to their respective locations in the initial conditions. The volume is then recentred on this region and the said region 'repopulated' with lower mass dark matter particles in concentric shells of increasing resolution. Each 'generation' of dark matter particles is 1/8 the mass of the previous generation. The highest resolution dark matter particles have a mass $9.5 \times 10^4\,\mathrm{M}_\odot$. Only within the high-resolution region are gas particles now placed, and tracked forward in time in a resimulation of the volume, now including the effects of star formation and feedback. These gas particles each have a mass $1.6 \times 10^4\,\mathrm{M}_\odot$; star particles which form from these gas particles have masses of $3.3 \times 10^3\,\mathrm{M}_\odot$. The force resolution within the inner, high-resolution, region is 150 pc. At redshift $z = 0$, there are 3.5×10^6 baryonic particles within the inner 20 kpc.

[3] Alternatively, the gas falling along filaments could change direction.

3 BASIC CHARACTERISTICS OF THE SIMULATED SYSTEM

As noted earlier, the simulation discussed here was first introduced by Brook et al. (2008), but a detailed examination of its dark matter halo characteristics, relationship to large-scale structure, stellar and gas-phase metallicity distributions, and their relationship to the system's proposed formation were reserved for future work. We address these points in what follows. A schematic of the system is shown in Fig. 1, where the older, 'primary', stellar disc is shown in colour (vertical in this figure) and the cold gas associated with the younger, 'secondary', polar disc is represented by the red contours (horizontal in this figure).

We can identify the polar and stellar discs cleanly via the ages of their associated star particles: recently formed stars ($t > 9$ Gyr) define the 'polar disc', while intermediate-age stars ($4 < t < 6$ Gyr) define the 'stellar disc'. This simple delineation is used to define the disc orientations for our subsequent analyses. Stars formed early ($t < 4$ Gyr) are associated with the halo of the galaxy and can be traced to the stars which formed before or during the last major merger.

The system as a whole has a dynamical (stellar) mass of $1.6 \times 10^{11}\,M_\odot$ ($1.0 \times 10^{10}\,M_\odot$) within its virial radius ($\sim$130 kpc) at $z = 0.17$. The stellar mass of the old stellar disc is $1.9 \times 10^9\,M_\odot$, while the polar disc has a mass of $9.8 \times 10^8\,M_\odot$, i.e. the polar disc has half the stellar mass of the stellar disc. The gas mass in the polar disc is approximately the same as the stellar mass at $z = 0.17$, so the baryonic mass in the two discs is approximately the same. Both discs are less massive than the very old spheroid (with stars formed at less than 4 Gyr which have a mass of $6.2 \times 10^9\,M_\odot$). Of the three polar ring galaxies studied in Spavone et al. (2010, 2011), two show a polar disc more massive than the host galaxy, while UGC 7576 has a polar *ring* 2.7 times less massive than the host galaxy. Our polar disc is 3.6 times less massive than the host, a value similar to that found for UGC 9796 by Spavone et al. (2011). The similarity in the masses of the two discs differs from NGC 4650A (Spavone et al. 2011). These mass values are highly dependent on the age cuts used to define the disc. The original values from Brook et al. (2008) give significantly different mass values for the two discs and so the relative mass of the two components is mostly dependent on how one chooses to define it, rather than an intrinsic property. For example, if we decompose using the method of Abadi et al. (2003)[4] then the stellar masses of each disc are the same, so that the total baryonic mass of the polar disc is twice that of the stellar disc.

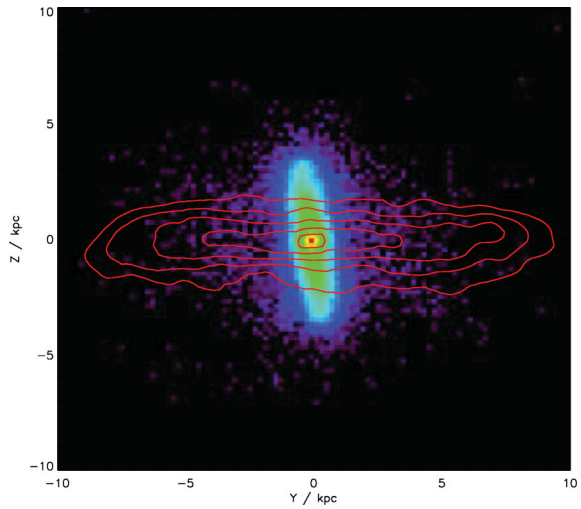

Figure 1. Schematic density distributions of the intermediate-age stars associated with the primary stellar disc (colours; vertical in this plane) and cold gas associated with the secondary polar disc (contours; horizontal in this plane).

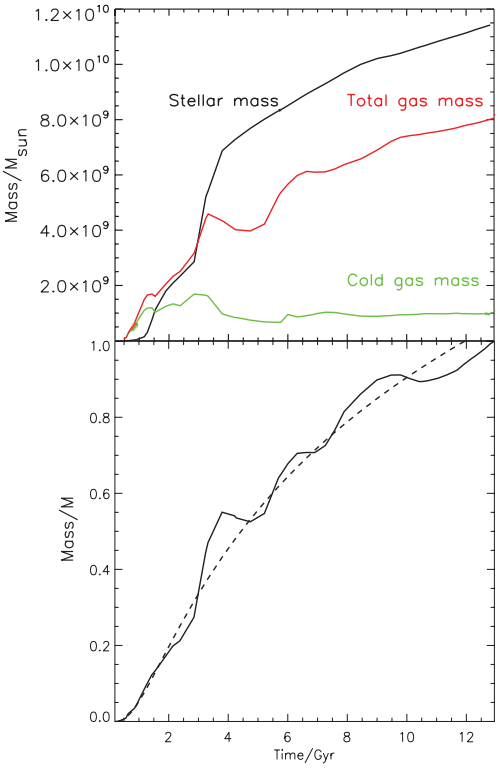

Figure 2. The upper panel shows the mass accretion of the baryonic components, with galaxy mass against the age of the universe. The bottom panel shows the dark matter accretion history, where the dotted line is the best-fitting (Wechsler et al. 2002) function.

The stellar disc is essentially gas free by redshift $z \sim 0.2$, but prior to this, there is an extended period of time during which there is gas in both discs. The scale-lengths of the stellar and polar discs are 1.0 and 3.4 kpc, respectively, with both showing disc truncations near $\sim$3 disc scale-lengths. The two discs are nearly orthogonal, with an inclination of $\sim 84^\circ$ between the two. The circular velocity at 2.2 scale-lengths for both discs is $\sim$110 km s^{-1}, based on the Brook et al. (2008) analysis. The polar disc system reported by Macciò et al. (2006) possesses similar masses and radial extents for its two discs. We show the mass accretion history of the galaxy in Fig. 2. We can, in some sense, think of this history in terms of three epochs of 'star formation': a rapid initial phase ($t < 4$ Gyr), an intermediate phase ($4 < t < 8$ Gyr) and a more gentle, later, phase ($t > 8$ Gyr).

3.1 History of formation

The primary disc first forms at redshift $z = 3.3$ (age $= 2$ Gyr) and the last major merger (with a mass ratio near 1:1) encountered at $z = 2.2$ (age $= 3$ Gyr). The interaction between the merging

[4] This galaxy is decomposed according to the ratio of $\epsilon = J_z(E)/J_{\rm circ}(E)$, where $J_z(E)$ is the z component of the angular momentum of the galaxy and $J_{\rm circ}(E)$ is the angular momentum of the circular orbit with the same energy E. Disc stars are chosen via a cut in ϵ close to 1.

galaxies lasts for ∼1 Gyr and significantly disrupts the primary disc, although the disc re-establishes itself rapidly due to its gas-rich nature. There is a delay between the last major merger and the time at which the polar disc becomes noticeable (at redshift $z = 0.8$, age = 6.8 Gyr). The polar disc then establishes itself, evolving passively and stably for the last ∼4 Gyr of the simulation. In the Brook et al. (2008) galaxy studied here, the polar disc component of the galaxy initially forms as a ring but over the following Gyr the centre is filled by cold gas to resemble a disc. For a video of the polar disc formation, first presented in Brook et al. (2008), see http://www.youtube.com/watch?v=c-H3WzaewdY. Only in the final ∼0.2 Gyr does the polar disc become unstable due to coupling between the two discs, and the polar disc structure vanishes when the two align. There is some evidence of a bar growing in the polar disc right up until the disc is disrupted, and a bar is evident in the old stellar disc as well. The surprising longevity of simulated polar disc structures was highlighted by both Macciò et al. (2006) and Brook et al. (2008). The former note that only gas which falls into the polar disc at ∼90° to the massive stellar disc can form a stable secondary disc; at smaller angles of incidence, the infalling gas was found to fall rapidly to the already existing disc.

3.2 Star formation history

The polar disc system experiences a fairly constant, intense, phase of star formation between 1 and 4 Gyr after the simulation commenced (Fig. 3). Subsequent to this, the global star formation decreases rapidly for the final ∼8 Gyr of the simulation (dashed black curve). We can infer the star formation histories along each disc by placing 'slits' along each (with the knowledge that by doing so means some 'duplication' of star formation histories in the region of overlap between the slits). Although we use the two discs to define where we place the 'slits', we include all stars along the 'slit' in our determination of the SFR. The result of this suggests that the primary stellar disc forms its stars preferentially at early times, prior to the last major merger, although residual gas does remain to form stars at later times (solid black curve). Over the final ∼5 Gyr of the simulation, stars start to form in the polar disc (solid red curve; see also fig. 2 of Brook et al. 2008), increasing steadily, while the star formation in the primary stellar disc has essentially halted over the final ∼4 Gyr. During this era, the star formation in the polar disc is very smooth and continuous, with no starburst features indicative of merging events. Star formation is ongoing and increasing, up to $z = 0.17$, but there is no sign of bursting, with a considerable fraction of stars being produced recently, so we expect young stars in the polar disc, as in NCG 4650A (Gallagher et al. 2002), although no spiral can be seen such as in NGC 4650A. Star formation is uniform throughout the disc, so there are no young star cluster regions, merely global star formation without clumping. This does not, however, mean that the SFR is similar to UGC 7576 or UGC 9796, which Spavone et al. (2011) fitted with an exponentially decaying SFR. Indeed, the SFR in the polar disc is increasing with time. The residual star formation not accounted for between the dashed curve and the sum of the two solid curves is that associated with the spheroid components of the system. In Fig. 3, the dotted line (representing 10 per cent of the global SFR) shows that the star formation within the discs (the 'in situ' component) is a small fraction of the global star formation at early times.

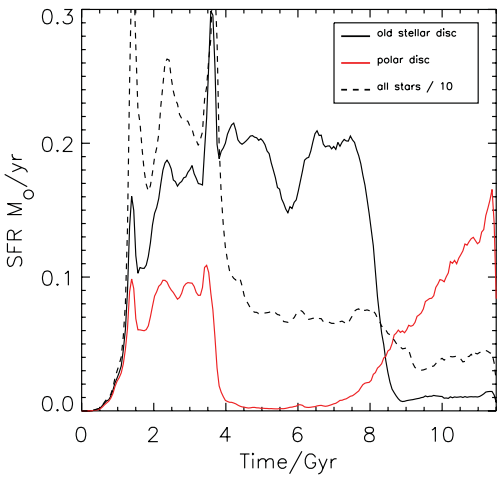

Figure 3. Time evolution of the SFR of the simulated system. The solid black line shows the SFR inferred from stars presently situated within a slit aligned with the old stellar disc and excluding the first kpc; the solid red line corresponds to the SFR inferred from a slit aligned with the polar disc; the dashed line corresponds to the global SFR of the system scaled down by a factor of 10.

As noted in Section 3, the system was decomposed using a stellar age cut: stars formed after $t > 9$ Gyr are considered as part of the polar disc, and those formed before that are assigned to the stellar disc.

4 THE HALO

One of the original reasons for postulating the existence of dark matter was the circular velocity profiles of galaxy discs. With polar discs, we have circular velocities of two orthogonal components of the dark matter density profile and so these objects provide an ideal method for studying the shape of the dark matter halo, as highlighted by Combes & Arnaboldi (1996), Casertano & van Gorkom (1991), Schweizer et al. (1983), Sackett et al. (1994) and Iodice et al. (2006); indeed, making use of the Tully–Fisher relation, as applied to polar discs, Iodice et al. (2003) suggested that dark matter haloes are oblate and flattened along the polar disc because the H I gas polar disc was found to have a faster circular velocity than the stellar disc.

In calculating the shape of the dark matter halo directly, we use the method of Knebe et al. (2010). The shape of the halo is calculated using spherical shells; at each radius, R_i, we calculate the inertial tensor using all particles within that radius. We use the standard inertial tensor, as opposed to the reduced tensor, because this technique strongly biases the profile in favour of the central region.

The halo shape is calculated, according to the inertial tensor, as

$$I_{i,j} = \sum_n = m_n x_{i,n} x_{j,n}, \tag{1}$$

where $I_{i,j}$ is the inertial tensor, n is the particle id, i and j are the x, y, z components of the particle position vector. The axial ratios are $(a, b, c) = (\sqrt{\lambda_a}, \sqrt{\lambda_b}, \sqrt{\lambda_c})$, where $a > b > c$ and $\lambda_{a,b,c}$ are the eigenvalues of the tensor. The directions of the axes are the corresponding eigenvectors, as outlined by Bailin & Steinmetz (2005).

This method easily identifies the direction of the principal axes of the best-fitting ellipse, but introduces a bias in the halo shape. To correct this to match halo sphericity based on potential energy contours, we must adjust the sphericity parameter, $S = c/a$, by

$$S_{\rm true} = S_{\rm sphere}^{\sqrt{3}}, \tag{2}$$

where the sphericity is the ratio between the major and minor axes of the halo. This relation is based upon the study by Bailin & Steinmetz (2005).

We will compare our inferred halo shape with that of Macciò et al. (2006), in addition to the work of Bailin et al. (2005), who studied the alignment of traditional galaxy discs with their dark matter haloes and found that in the inner region there was a tight alignment which becomes increasingly divergent with distance. Thus, we have the amount of mass within a radius R along two orthogonal directions, M_1 and M_2.

In order to calculate the axial ratios, we imagine two spheres of radii 'a' and 'b', containing the same mass. The ratio of the volumes of these two spheres is the same as the ratio M_2/M_1. Therefore, the axial ratios of the halo are $(M_2/M_1)^{1/3}$.

4.1 Radial profile

Using the inertial tensor approach outlined above, in Fig. 4 we show the sphericity profile of the system's dark halo (upper panel) and the direction of the minor axis of the inertial tensor (bottom panel) as a function of galactocentric distance. We find the system is embedded within a nearly spherical ($S = 0.9$) halo near the edge of the stellar disc (∼5 kpc), but which declines in sphericity both within the inner kpc and beyond ∼10 kpc. This reaches a minimum sphericity at 54 kpc or approximately half the virial radius and increases again to a final value of 0.67 at $R_{\rm vir}$. The dark halo is prolate at the edge of the stellar disc, distinctly oblate at about 15 kpc and then becomes increasingly triaxial. No obvious 'imprint' of the polar disc is seen in the sphericity profile.

This sphericity trend is similar to that of the Macciò et al. (2006) galaxy, which has an inner region of greater sphericity than the outer region. This will be discussed further later in this section.

In the bottom panel, we can see that the direction of the halo's minor axis in the innermost region is orientated 90° to the minor axis in the outer region. The inner region is flattened against the direction of rotation of the stellar disc and the polar disc is aligned to the axis of rotation of the stellar disc. The polar disc has been aligned to the z-axis of the volume and the stellar disc is approximately aligned to the y-axis. Thus, it is clear that the minor axis of the halo in the innermost region is aligned to the stellar disc and in the outer region it is aligned to the polar disc.

For non-polar disc galaxies, the minor axis of the dark matter halo is found to align closely with the angular momentum of the

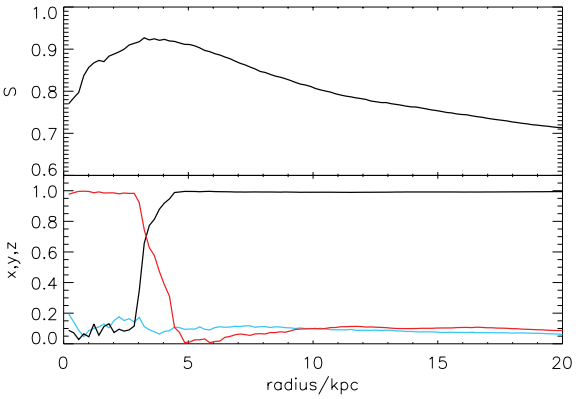

Figure 4. Upper panel: the sphericity profile of the dark matter halo as a function of galactocentric distance. Bottom panel: the direction of the minor axis of the inertial tensor (black: z-component; red: x-component; cyan: y-component).

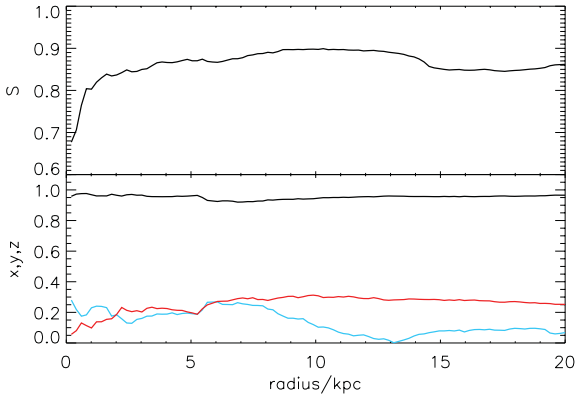

Figure 5. Top panel: the sphericity profile of the dark matter halo as a function of galactocentric distance, for a simulated 'classical' disc galaxy. Bottom panel: the direction of the minor axis of the inertial tensor (black: z-component; red: x-component; cyan: y-component).

disc (e.g. Bailin et al. 2005). Fig. 5 shows an example of such a non-polar disc galaxy (g15784 from Stinson et al. 2010). This galaxy shares some similarities with our polar disc galaxy in that it has not experienced a merger or starburst for the past ∼4 Gyr. From the bottom panel, one can see that there is no sign of the obvious twist in the minor axis profile (cf. Fig. 4, for the polar disc system here), consistent with the conclusions of Bailin et al., thus demonstrating a significant difference in the properties of the two dark haloes.

Another feature of the dark haloes of the Bailin et al. (2005) sample of eight galaxies is that although the disc angular momentum and dark halo minor axis are tightly aligned in the centre, they diverge with increasing radius. The dark halo of the polar disc galaxy seems to remain closely aligned at large radii outside the twisted region. Such behaviour is seen in only one of the eight galaxies in the Bailin et al. sample. This may be a coincidence, but this strong behaviour in an object that is itself uncommon may hold additional clues as to the physics by which the polar disc formed. A larger sample size is required to exclude the possibility of chance.

Iodice et al. (2003) note that polar disc galaxies have an offset from the Tully–Fisher relation relative to other spiral galaxies, showing faster rotation for a given magnitude. This is indicative of flattening of the potential towards the plane of the polar disc, as we have demonstrated above. Our polar disc galaxy ($M_I = -20.3$; $B - I = 1.7$, from table 1 in Brook et al. 2008; this is for the whole galaxy as in Iodice et al. 2003), when compared with the Tully–Fisher relation of S0 galaxies (Williams, Bureau & Cappellari 2010), lies above the best-fitting line, but not significantly so. Considering that Williams et al. (2010) note that the Tully–Fisher relation for S0s is lower than that of spirals, the polar disc galaxy should actually be indistinguishable from these standard populations, as we find when we compare our stellar mass and circular velocity to the results of Pizagno et al. (2005) and McGaugh (2005), among others. This is not unexpected as only seven of the 16 galaxy sampled by Iodice et al. (2003) are exceptionally displaced from the general Tully–Fisher profile in their paper. A larger sample of simulated polar discs would be required to develop any further conclusions in this area, together with a larger sample of K-band observations of polar ring (or disc) galaxies.

Macciò et al. (2006) studied the shape of a simulated polar disc galaxy and calculated the sphericity of the galaxy halo as we have done here. There are some differences. Their shape profile peaks at a sphericity of approximately 0.8, at a radius of 9.8 kpc. Our polar disc peaks at a sphericity of 0.93 at only 3 kpc, corresponding to

the edge of the stellar disc. At half the virial radius, our halo is still more spherical than was found by Macciò et al. (2006) with a sphericity of 0.65 compared to their 0.5. Our values are fairly stable with redshift during the lifetime of the polar disc. This galaxy has a sphericity peak at approximately twice the inner disc, unlike in our galaxy where the peak and the edge of the stellar disc coincide. The sphericity peak in Macciò et al. (2006) is 0.8 compared to our 0.9 and at half the virial radius the sphericity is 0.5, again less spherical than for our polar disc. Without further comparison in the shape-finding methods, and a larger statistical sample, further conclusions cannot be drawn.

4.2 Evolution

We analysed both the classical disc galaxy from Fig. 5 and the polar disc galaxy towards the ends of their respective quiescent phases (∼4 Gyr after the last significant merger/burst of star formation, or post-establishment of the polar disc, respectively). The direction of the minor axis of the polar disc's dark halo is strongly aligned with the same plane (the z-axis of the polar disc angular momentum) for much of the simulation (Fig. 6). This is not the case for the classical disc, where the minor axis changes significantly from redshift $z = 0.3$ (age = 10.3 Gyr) to $z = 0$. Thus, there appears to be a strong, long-term alignment in the shape and direction of the polar disc halo. This strong alignment may be important in giving rise to the polar disc, but we are hindered by our sample of only one galaxy in coming to a strong conclusion on this point.

The inner region of the polar system shows a long-term 'twist' that evolves towards orthogonality. The classical disc, after the last starburst, sees an evolution towards alignment throughout the halo, such that no twist is evident. We suggest that the initial misalignment is due to the merger of infalling subhaloes temporarily reorienting the disc, and the alignment thereafter is traced to the later quiescent phase. This raises the interesting possibility that alignment of the galaxy and dark halo is due to the torques on the galaxy by the dark halo. Bailin et al. (2005) discounted this, although they did find that the disc is always aligned with the inner halo, which we find not to be the case, at least for part of the lives of both discs. For our polar disc system, the orientation of the dark matter halo in the outer region is set early and does not significantly change over the course of the simulation. The classical disc shows considerable variation in the direction of the halo minor axis from 0° to 90° over time.

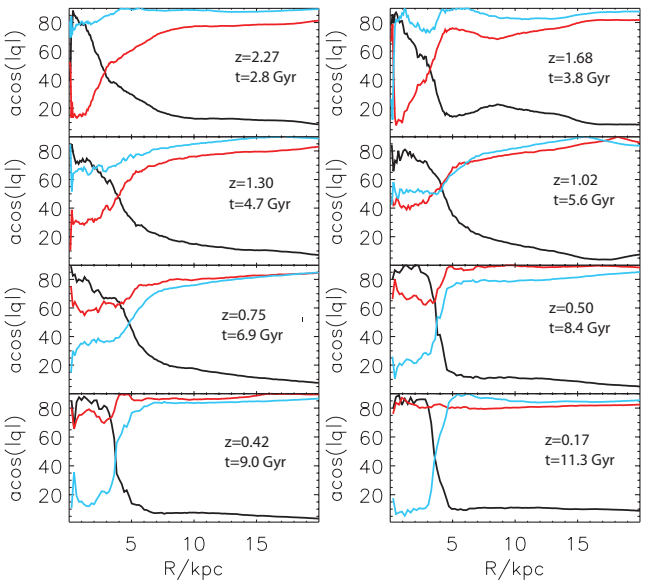

Figure 6. Time evolution of the alignment profile of the halo's minor axis with the simulation aligned to the polar disc. The black line is for the z-axis (parallel to the polar disc angular momentum), the red line for the x-axis, and the cyan for the y-axis (approximately parallel to the stellar disc angular momentum at $z = 0.17$). The ordinate for each panel is the arccosine of the modulus of the projection of the minor axis along each of the principal axes. The y-axis is defined as the angle of the minor axis relative to the z-axis of the angular momentum of the cold gas.

4.3 Shape from observations

In order to derive the shape of the polar disc halo from observational data alone, we can take measurements of the circular velocity of each disc. This is best done from the edge-on view because it becomes difficult to identify these galaxies simply because of orientation effects (Whitmore et al. 1990). By measuring the circular velocity of the two discs edge-on, we can gain insight into the shape of the dark halo.

First, we derive the line-of-sight velocity profiles of the two discs by, again, laying down 'slits' along both. These profiles can then be used to infer the enclosed mass as a function of galactocentric radius. If the inferred mass along one disc is greater than that inferred along the orthogonal slit, the former is likely the direction of the major axis. We use the aforementioned redshift $z = 0.17$ snapshot [the point at which the two discs are near the end of their ∼4 Gyr stable period and highly orthogonal (86°)] to undertake this analysis. We arbitrarily assign SPH particles with temperatures $T < 40\,000$ K to be 'cold gas', although our analysis is not sensitive to this choice. For the stellar disc, we concentrate upon stars we know to be rotationally supported which were formed between 6 and 6.5 Gyr after the start of the simulation, in order to minimize contamination from the old centrally concentrated disc+bulge stars, the stellar halo and the polar disc itself. Using the circular velocity ($v_{\rm circ}$) and the galactocentric radius (r), we calculate the mass within that radius (M) as

$$M(< r) = \frac{v_{\rm circ}^2 r}{G}, \tag{3}$$

where G is the usual gravitational constant.

Using the circular velocity profiles of the two orthogonal discs, we can probe the dark matter halo using observationally measurable galaxy properties. We show the velocity and enclosed mass profiles of the discs in Fig. 7 (top and bottom panels, respectively). If there is more mass within a distance r of the centre of the galaxy, then the halo is compressed in that direction. From the bottom panel of Fig. 7, we can see that there is more mass *along* the stellar disc than the polar disc, which corresponds to a halo compressed orthogonally to the polar disc. At 3 kpc the difference in mass is ∼70 per cent, with the mass along the stellar disc being greater. Taking the cube root of the mass, to crudely estimate the axial ratios, gives 0.9, which matches remarkably well with the direct computation of the halo shape, which was found to be 0.92 (Fig. 4), confirming the validity of using the two discs to probe the shape of the halo.

Brook et al. (2008) note a very high V/σ relation of 4.4 for the stellar disc and 1.4 for the polar disc. This matches well with the high V/σ seen in observations, e.g. Schweizer et al. (1983) who calculate a V/σ of 2.2 for A0136-0801 and Spavone et al. (2011) who give $V/\sigma = 1.8$, 2.15 and 1.28 for UGC 7576, UGC 9796 and NGC 4650A, respectively.

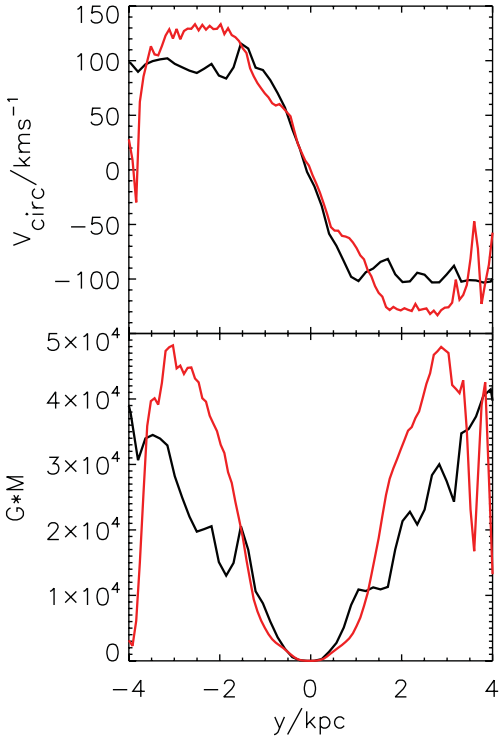

Figure 7. Top panel: line-of-sight velocity profile for the intermediate-age stars (red line) and the polar disc cold gas (black line) at redshift $z = 0.17$ (age = 11.6 Gyr). Bottom panel: enclosed mass as a function of radius based upon equation (3).

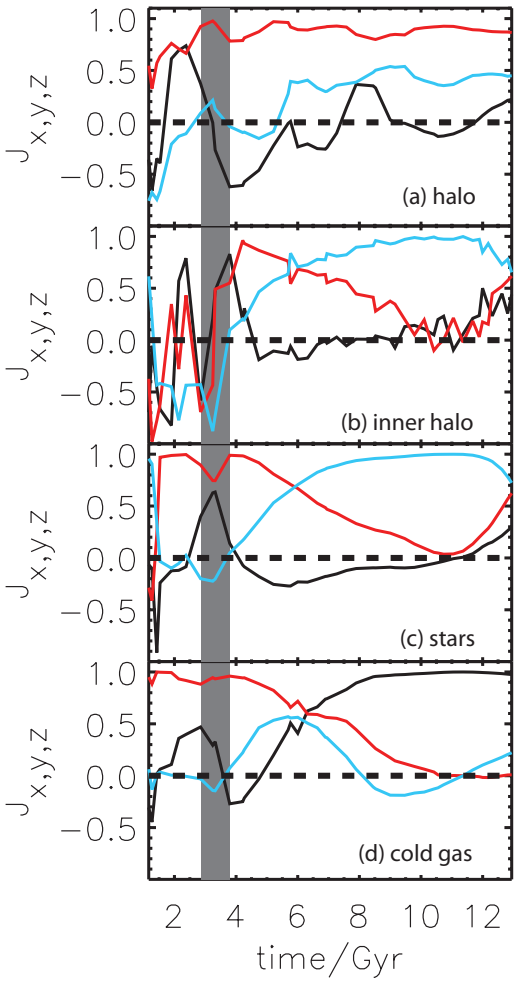

Figure 8. Normalized angular momentum projected on the three principal axes of the simulation volume: black shows the z-axis, red the x-axis and blue the y-axis. The top panel, labelled 'halo', is the angular momentum of the entire halo; the panel labelled 'inner' is the angular momentum of the inner kpc of the halo; the panel labelled 'stars' is the angular momentum evolution of old ($t < 3$ Gyr) stars; the panel labelled 'cold' shows the trend for the cold gas. The grey area is the time of the last major merger.

5 FORMATION AND EVOLUTION

5.1 Angular momentum

In order to understand the processes that give rise to the polar disc, we examine the evolution of the angular momentum of the gas, stars and dark matter. Although not directly related to the disc structures, the effect of dark matter is important because of the effect of tidal torques.

In order to explore the formation processes of polar disc systems, we next traced the origin of the gas that lies within the system and formed stars in the discs. Maccio et al. (2006) point out that unless the infall of gas is along the polar axis of the potential, it will be dragged to align with the stellar disc potential. When gas collapses under gravity it retains angular momentum, and thus, the gas which comprises the polar disc and the stars of the stellar disc at $z = 0.17$ should have a different origin. Two possible origins of the polar disc galaxy are suggested: first, the gas that comprises the two discs falls along two different trajectories with two different angular momenta, or secondly, the last major merger was inclined to the galaxy and so reoriented the existing gas and stars. New gas would then fall in along the old filament, but the early infall baryons would not be reoriented.

We align the simulation such that the polar disc at redshift $z = 0.17$ is aligned to the z-axis and use that orientation at each earlier time-step. The evolution of the angular momentum of the inner and outer dark matter halo, the gas and the stars is shown in Fig. 8. This plot shows that the alignment of the angular momenta of the old stars, intermediate-age stars, gas and dark matter experiences a constant evolution with time after 6 Gyr. The polar disc galaxy evolves continuously into its $z = 0.17$ (11.6 Gyr) position with no sharp transitions.

The angular momentum of the dark matter halo (panel a) is established early and remains essentially constant for the rest of the simulation, although some tumbling can be seen in the z-axis. The angular momentum of the entire halo remains essentially the same throughout the history of the simulation, especially the x-component. This matches with the shape of the dark halo in the outer regions, which remains essentially constant.

We see that the angular momentum of the inner region of the dark halo (panel b) and the stars are locked together because in this region the stars dominate the gravitational potential of the halo.

We have previously discussed that the shape of the polar disc halo, and its orientation, remains fairly constant with time. We can use the axes of the best-fitting ellipse at a radius of $0.25R_{vir}$ to calculate the cross-correlation of the gas and stars with the shape of the halo potential, as shown in Fig. 9.

The angular momentum of the polar disc aligns to the minor axis of the dark halo, as previously discussed, and the old stars align with the major axis within 2 Gyr of the last major merger. The cold

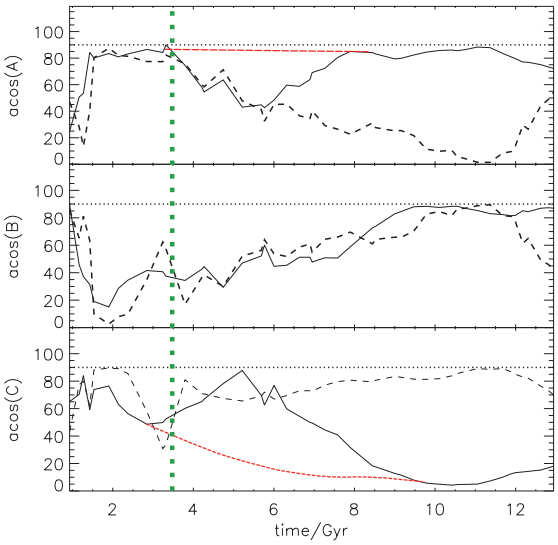

Figure 9. The angle between the angular momentum of the cold gas (solid line) and the old stars (dashed line) and the major (top panel), intermediate (middle panel) and minor (bottom panel) axes of the dark matter halo. The shape of the halo is measured at 0.25 $R_{\rm vir}$. The dotted green lines show the time of the last major merger for reference and the red lines indicate the angular momentum which the galaxy would presumably have followed without the last major merger occurring.

gas takes up to 4 Gyr to move into close alignment with the minor axis. This may be suggestive of interactions between the dark halo potential which follows the dark halo shape and the galaxy gas and stars.

The old stars (Fig. 8, panel c) move orthogonally to the cold gas (Fig. 8, panel d) after the last major merger. During the last major merger, there is a peak in the z-axis angular momentum of the stars which appears to have no long-term effect. This can be seen in both Figs 8 and 9. At this point, the other two axes begin to twist into their final redshift $z = 0.17$ (age = 11.6 Gyr) position.

A striking feature of Fig. 9 is that there is no difference in the orientation of the gas and stars along the intermediate axis in any given time period (middle panel). The cold gas angular momentum becomes increasingly aligned to the halo minor axis (bottom panel). The most notable feature from this plot is that the gas sees a temporary change in direction relative to the major axis (top panel) after the major merger, but recovers. The red line shows the assumed evolution of the gas angular momentum had the last major merger never occurred, although this has not been tested. The old stars, however, *do not recover* or regain their old angular momentum.

The angular momentum of the galaxy at early times is closely aligned with the intermediate axis of the halo inertial tensor but becomes increasingly divergent. The gas and stars are originally closely aligned but diverge after the last major merger. We see that initially the galaxy angular momentum is orthogonal to the major and minor axes and aligned to the intermediate axis. After the last major merger, there is a change in the angle of both components relative to the major axis that the old stars maintain. The infalling gas returns to orthogonality within several Gyr. Without the major merger it seems likely that the gas and stars would remain orthogonal to the major axis. There is, however, an evolution in the angular momentum relative to the intermediate axis, such that the gas and stars angular momentum is initially along this axis but then increasingly diverges. Had the major merger not disrupted the system, it seems likely that there would be a continuous evolution of both components until the galaxy angular momentum aligns to the minor axis in agreement with Bailin et al. (2005). This can be assumed from Fig. 9. The recovery time suggested corresponds to a feature of the total angular momentum of the cold gas. Although not shown in Fig. 8, the last major merger appears to result in an increase in the total angular momentum of the cold gas followed by a decrease which lasts from 4 to 6 Gyr. After 6 Gyr, the angular momentum of the gas rapidly increases again. The angular momentum of the old stars does not change in magnitude during this collision.

5.2 Formation process

The formation process of the galaxy is intimately connected with the evolution of the angular momentum described in the previous section. This is because the changing alignment of the galaxy with respect to the large-scale environment is what gives rise to the polar disc properties.

Another manifestation of misaligned gas and stellar discs can be seen in the phenomenon of warps. It is perhaps reasonable to assume that warps and polar discs might have a common origin. In this section, we first briefly examine the possibility that a polar disc is an extreme type of warp. We then test the formation scenario presented in Brook et al. (2008) by tracing the angular momentum evolution of the infalling gas and the direction of the last major merger.

Warps are now thought to be due to the interaction between infalling gas and misaligned hot gas (e.g. Roškar et al. 2010). In our simulated system, though, the hot gas is aligned to the polar disc. Warps begin at the truncation of the stellar disc and the gas is only misaligned to the stellar disc outside this radius (Sánchez-Blázquez et al. 2009). The polar disc at $z = 0.17$ (11.6 Gyr) is out of alignment at all radii and (essentially) perfectly orthogonal, suggesting that polar discs and warps are distinct processes. At first glance, there seems to be no significant similarity between warps and polar discs. However, there is evolution of the direction of the polar disc galaxy, as a whole, after the formation of the polar disc (Fig. 9), possibly due to tidal torques.

We identified gas that comprises the polar disc as all gas that is cooler than $T = 40\,000$ K within the inner 10 kpc of the host halo at $z = 0.17$ when the polar disc is most prominent. This lower temperature threshold does not change the direction of the angular momentum of the gas but results in a thinner, better defined, disc structure. We track these particles to their origin, then repeat the process tracing the gas that formed stars prior to the last major merger at $z = 2$. When we plot the positions of these sets of particles, there is little obvious difference between the two, which one might expect if the origin of the gas was different filaments.

If we examine an output from before the last major merger, we see that there is a broad range of angular momentum in the infalling gas which becomes systematically more aligned to the z-axis with time. The angular momentum of the infalling gas is surprisingly coherent with distance from the galaxy. The total angular momentum of the gas which forms the polar disc stars is tightly aligned with the z-axis from ∼4 Gyr onwards. It is a similar story if we exclude the gas which is already in the inner region (within the inner 1 kpc of the galaxy). This appears to confirm the Macciò et al. (2006) hypothesis regarding the importance of cold flows along filaments for polar disc galaxy formation.

Another feature of the polar disc structure is that during intermediate times the star formation in the old stellar disc is fuelled by newly infalling gas. The reason for this is that when gas falls into the innermost region of the galaxy it is strongly affected by the already

formed stars, which changes the angular momentum of the gas and brings it into alignment with the stellar disc. In the inner region, the potential is dominated by the stars. An observational confirmation of this is Combes & Arnaboldi (1996), who find that no dark halo is needed to reproduce the rotation curve of the stellar disc in NGC 4650A.

This behaviour no longer occurs after about 9 Gyr. As the entire galaxy is gradually rotating to bring it into alignment with the galaxy halo shape, it may be that the gas is at a steep enough angle to the stellar disc so that it is no longer dragged into alignment with the stellar disc at later times. This is suggested by Macciò et al. (2006) as to why infalling gas needs to be approximately orthogonal for a polar disc to be stable.

We also see that a considerable fraction of the gas which forms the polar disc is aligned to the z-axis when it is still far from the galaxy, but by no means all the gas is tightly aligned, and interactions within the galaxy halo are important in finally aligning the gas.

The scenario favoured by Brook et al. (2008) suggested that the polar disc galaxy is formed if the last major merger has a total angular momentum orthogonal to the infalling gas. This interaction reorientates the old gas and stars, while the angular momentum of newly infalling gas remains unchanged. The coincidence of the last major merger with the more unusual behaviour of the angular momentum (Fig. 8) of the galaxy is suggestive that it is essential to the formation of the galaxy. The mass of stars in the polar disc galaxy at $z = 2$ is 3.2×10^9 M$_\odot$ and the merging satellite galaxy is 1.5×10^9 M$_\odot$, making the interaction at least 1:2.

The angular momentum of the collision is calculated by assuming that each galaxy is a point sitting within the reference frame of the infalling gas. The relative tangential motion of the collision is anticlockwise. A schematic example of the galaxy–galaxy interaction is shown in Fig. 10. By examining the internal angular momentum of the interacting galaxies, we found that most of the angular momentum of the interaction is stored in the bulk motion of the galaxies rather than in internal motions. The angular momentum of the satellite's stars is aligned to the angular momentum of the merger.

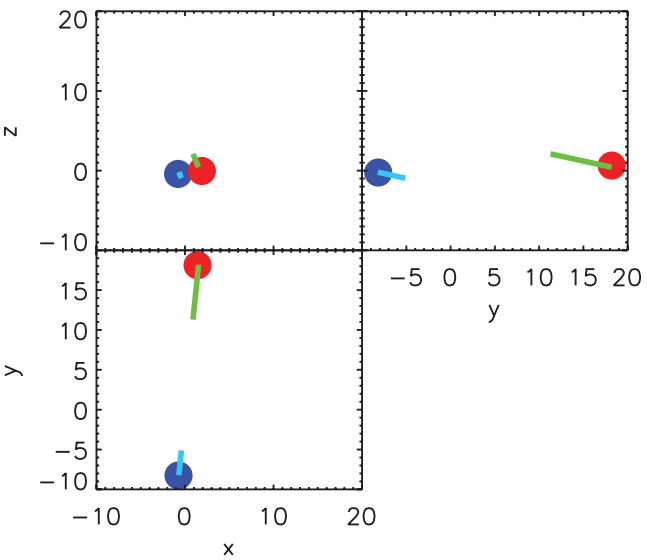

Figure 10. Projected schematic of the last major merger at redshift $z = 2$ (age = 3.3 Gyr), just before the stars merge. The blue star is the central galaxy, while the red star is the galaxy which merges. The blue and green lines are the projected velocity vectors. Distances are in kpc.

The angular momentum of the collision is along the x-axis in the chosen reference frame. This is orthogonal to the angular momentum of the gas falling into the halo from the filament which is aligned to fall in along the z-axis. As the angular momentum of the system must be conserved, we suggest that this provides the *initial* kick which reorients the old stars away from the initial orientation (see Fig. 9). This figure suggests that the major merger alters the behaviour of the galaxy away from a matched gas and stellar disc which reorientates from being aligned to the halo intermediate axis to the minor axis.

Much of the gas that forms stars between 4 and 6.5 Gyr has its origin in the satellite galaxy involved in the last major merger, and thus contributes greatly to the alignment of the stellar disc. Specifically, 40 per cent of the stars formed between 4 and 6.5 Gyr were produced from gas which fell in with the last major merger.

The motion of the system after the major merger may be due to slow tumbling or torquing by the halo as mass continues to be accreted. This is important because the stellar disc eventually aligns with the y-axis of the system.

5.3 Metallicity and age

We derived the radial (mass-weighted) metallicity gradients of the discs associated with our simulated polar system by placing narrow slits along each component, ignoring the innermost 1 kpc of both, to avoid bulge contamination and the intersection point between the two. The overall stellar metallicity of the stellar disc is roughly twice (four times) that of the polar stellar (cold gas) disc.

Fig. 11 shows the radial metallicity profiles for the intermediate-age stars of the stellar disc (black) and the cold gas of the polar disc (red). The metallicity gradient of the latter is very flat ($\sim -0.005 \rightarrow -0.01$ dex kpc^{-1}), consistent with the recent observation of flat gradients in NGC 4650A by Spavone et al. (2010). The metallicity gradients of the stellar and polar discs are -0.09 and -0.04 dex kpc^{-1}, respectively. This matches the results of Spavone et al. (2011), who find that the profile for UGC 7576 is also extremely shallow.

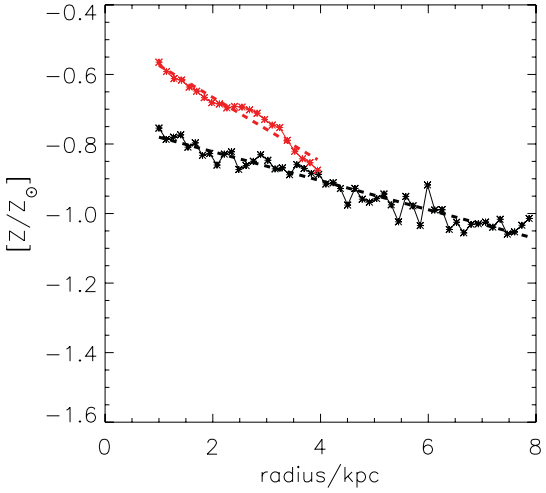

Figure 11. Radial mass-weighted metallicity profile for the stars formed in the primary stellar disc (red), and the cold gas of the secondary polar disc (black), along 1 kpc thick slits. The stellar disc truncates at ∼4 kpc; beyond that point, star particles are kinematically associated with the stellar halo. The polar disc truncates at ∼8 kpc. The dotted lines are the best-fitting lines to the metallicity profiles, where $[Z/Z_\odot] = mr + c$, m being the gradient in dex kpc^{-1} and c the y intercept.

The negative metallicity gradient seen in Fig. 11 is characteristic of inside-out disc growth (Matteucci & Francois 1989; Matteucci et al. 1989; Boissier & Prantzos 1999; Pilkington et al. 2012), consistent with the formation scenarios suggested by Maccio et al. (2006) and Brook et al. (2008) for their simulated polar disc systems. We did, however, note that the gas in the polar disc initially forms a ring at larger radii and then later 'fills in' the inner region. This is because while the polar disc is forming, the gas in the inner region is inclined to the old stellar disc rather than the developing polar disc, depleting the inner region of the polar disc structure. We suggest that the abundance gradient is indicative of the stellar disc enriching the gas in the inner region of the polar disc rather than polar disc stars alone. The lower metallicity polar disc is consistent with its younger age sampling an earlier part of the age–metallicity relation. It is consistent with a polar disc being preferentially 'polluted' by the infall of 'primordial' gas flowing into the system at late times along filaments. When we track the origin of this gas below, we confirm that this is indeed the case.

In terms of global metallicity, this polar disc galaxy is similar to those surveyed by Spavone et al. (2010, 2011). Specifically, $Z/Z_{\odot} = 0.2$ for our galaxy, matching the metallicity of NGC 4650A, higher than UGC 9796 ($Z/Z_{\odot}= 0.1$) and lower than UGC 7576 ($Z/Z_{\odot}= 0.4$).

The radial age profile of the stars along each disc shows that the stars are significantly younger in the polar disc than in the stellar disc (Fig. 12). The older spheroid component tends to dominate at both low and high radii, driving the declines seen at the extrema of both curves. If we remove stars that formed in the first ∼4 Gyr of the simulation, we find a flat stellar age gradient in both the stellar and polar discs. The mean formation time of stars in the stellar (polar) disc is 5–6 Gyr (∼10 Gyr) from the start of the simulation.

Looking at Fig. 3, we see a much higher SFR than is found by Spavone et al. (2011). However, their SFR matches that for our polar disc at 9 Gyr or about 1 Gyr after it begins to form. This is a similar age to the estimated age of the polar disc in NGC 4650A.

As part of our examination of the temporal evolution of the angular momentum, we looked at an alternative approach to decomposing the two discs, aligning the simulation volume using the cold gas distribution and calculating the angular momentum of each star particle. We can then plot the ratio of the z- and y-components of the angular momentum to the total angular momentum, as shown in Fig. 13. It is notable that the angular momentum of stars in the polar disc is tightly correlated with the gas, such that all stars with a J_z/J_t greater than 0.9 are considered part of the polar disc. For the stellar disc, the distribution is broader, suggesting stars with J_y/J_t greater than 0.75 are part of the stellar disc.

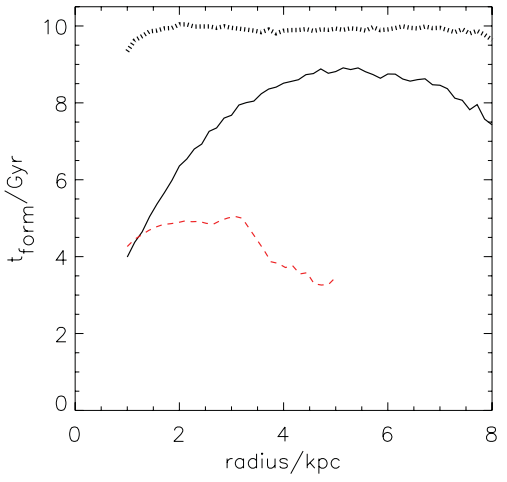

Figure 12. The stellar age profile along the polar (black) and stellar (red) discs. t_{form} is the mean formation time of stars at a given radius. The stellar (polar) disc truncates at ∼4 kpc (∼8 kpc). The black dotted line shows the star formation time with radius for the polar disc, discounting old stars ($t_{form} < 4$ Gyr).

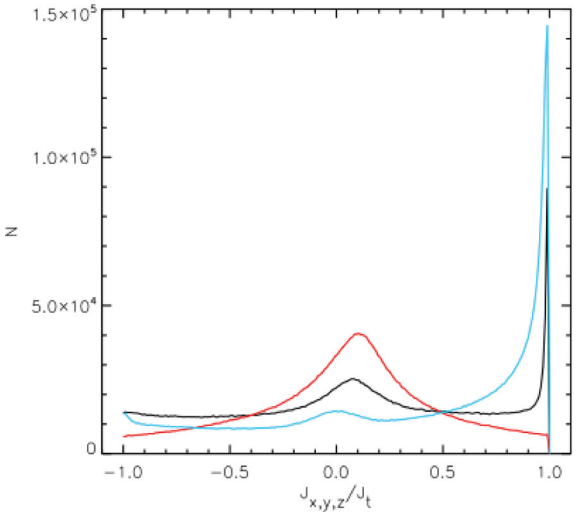

Figure 13. The angular momentum profiles of stars along the x (red), y (blue) and z (black) axes, where the cold gas has been aligned with the z-axis.

The above provides an age-independent method to identify the two discs using angular momenta without the age cuts used previously. This allows us to see how the discs grow; we bin the stars according to their distances along their respective discs. If we repeat the calculation of the stellar age profile using this new method, we can see that the slope at radius <4 and >6 kpc is apparently due to contamination from the bulge and stellar halo, respectively. This shows that there is no significant difference in the ages of stars at different radii, despite the presence of metallicity gradients.

Fig. 14, panel (a), shows that the star formation history of the polar disc changes slightly with radius, while panel (b) shows the same plot for the older disc. In the polar disc, panel (a) shows that there is a population of stars which forms early, contaminating the sample. Indeed, if we remove those early-forming stars ($t_{form} < 4$ Gyr) from the age profile, then the age gradient is almost completely flat, as if we were using the decomposition method discussed directly above. The black dotted line in Fig. 12 shows this trend. In Fig. 11, we show the *gas* metallicity gradient for the polar disc. When we trace the gas back in time, and identify it just before it enters the inner region (radius <12 kpc), we find that the metallicity gradient of the infalling gas is considerably flatter than at $z = 0.17$. This is based on the radius of the particle at $z = 0.17$ not the radius at the time of infall. Additionally, we find no particular gradient in the time at which the gas entered the inner region. This suggests that the reason for the metallicity gradient at $z = 0.17$ is the enrichment of the gas in the inner region due to a higher SFR at small radii, which is uniform across time. The metallicity gradient is, apparently, not indicative of an inside-out formation of the polar disc.

The metallicity distribution of the polar disc stars has the same gradient as the cold gas if we remove the very old stars, but the stars are 0.15 dex less rich at any given radius. If we include the old stars, then we find that the inner region is considerably more metal rich.

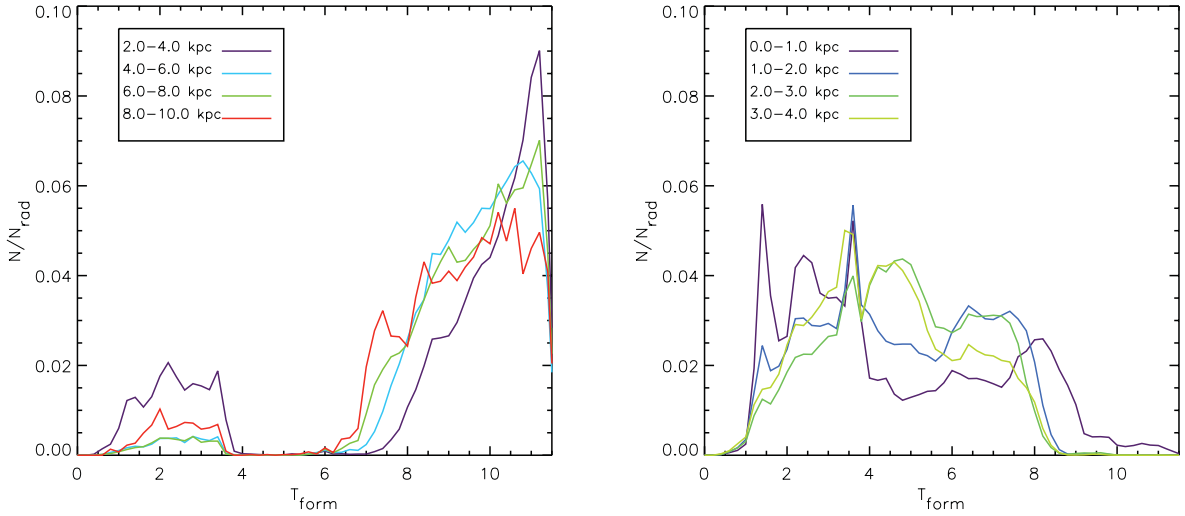

(a) Polar disc (b) Stellar disc

Figure 14. Age distribution of stars at different radii along each disc. The lines are colour coded as stated in the inset to each panel. (a) shows the polar disc stars, while (b) shows the stellar disc stars.

We conclude that the Brook et al. (2008) polar disc is comparable to the polar disc galaxies observed in nature (Iodice et al. 2002; Spavone et al. 2010). The polar disc structure is older than the value derived for NGC 4650A by Spavone et al., but has a comparable mean metallicity. The stellar disc is more metal rich than the younger polar disc, and the metallicity gradient for the polar disc is comparably shallow to that observed in NGC 4650A. The polar disc does not produce stars for ∼3–4 Gyr after the last major merger, consistent, for example, with the picture proposed for UGC 9796 (Cox et al. 2006).

6 CONCLUSIONS

We have extended the preliminary analysis of the polar disc structure first introduced by Brook et al. (2008). We have examined the properties of the dark matter halo shape, the formation process of this object and the metallicity and stellar age gradients of the discs.

Iodice et al. (2003) point out that polar disc galaxies provide an unparalleled chance to study the shape of the inner region dark matter haloes using observations in a way normally only possible in simulations. The two orthogonal discs have a circular velocity defined by the potential, which is dominated by dark matter. By comparing the circular velocity of orthogonal discs, we estimate the flattening of the dark matter in the plane where both discs are seen edge-on and find that the halo is flattened in the direction of the polar disc, as found by Iodice et al. Specifically, the axial ratio is found to be $c/a = 0.9$. Directly measuring the dark matter halo in the simulation, we find the same result and find the axial ratios are extremely similar using both methods, i.e. $c/a = 0.93$. The value quoted is for the inner region of the halo, at the radius of the polar disc itself. In the outer region of the disc, the sphericity declines to 0.67. We concentrated on the inner region in this work because that is the region probed by the baryons.

This value is closely matched by simulations of dark matter haloes, such as the galaxy size haloes with cooling simulated by Kazantzidis et al. (2004) and shown in their fig. 2, which shows an almost spheroidal inner region, with a sphericity of 0.9 at 10 per cent of the virial radius, and an outer region of $c/a = 0.6$, confirming the work of Springel, White & Hernquist (2004) and Allgood et al. (2006), amongst others. Allgood et al. (2006) has categorized halo shapes from cosmological simulations using statistical samples. Using their results, we expect our halo to have a c/a ratio of approximately 0.65 at $z = 0.17$, which is consistent with the polar disc galaxy halo; the value of c/a for the 'classical' disc shown in Fig. 5 at the viral radius is 0.7. The shape profile, both in angle and sphericity, remains stable from outside the inner region to the virial radius. This differs from the work of Bailin et al. (2005) and Allgood et al. (2006), who find a change of angle and shape with radius. This feature is unusual but polar discs are unusual objects and this may be characteristic. Macciò et al. (2006) did not see the same level of coherence in their polar disc galaxy, however.

Compared to observational estimates, e.g. Sackett (1999), however, these haloes appear very spherical. Studies of polar ring/disc galaxies (see Sackett et al. 1994; Combes & Arnaboldi 1996; Iodice et al. 2003) suggest a highly flattened halo of between 0.3 and 0.4. Sackett (1999) does, however, provide some suggestions as to why this difference occurs. Estimates of c/a for haloes based on different observations vary wildly depending on the chosen metric, such that $c/a = 0.5 \pm 0.2$. In the outer region of the halo the axial ratio (c/a) falls within this range with a value of 0.65. In the inner region ($R < 15$ kpc) where the observational estimates probe we see $c/a =$ 0.9–0.75. The simulation outcome is also close to the result of Hoekstra, Yee & Gladders (2004) based on weak lensing, who estimate a halo sphericity of $0.67^{+0.09}_{-0.07}$, the upper range of which is close to the sphericity of our halo at a radius of 14 kpc. As for the extremely elliptical shape found for polar ring/disc galaxies, the methods used may simply not give good estimates; indeed, Sackett (1999) notes the difficulty in measuring halo sphericity observationally.

We have concluded that the polar disc of this system is not caused directly by a merger or stripping. There is no single merger or stripped satellite which contains enough gas to form the massive polar disc. By process of elimination, the polar disc must form from inflowing cold gas, as in Maccio et al. (2006). We attempted to identify the mechanism by which this cold gas flows into the system and gives rise to the polar structure, asking why the filaments

should change direction relative to the old stellar disc. The structure of the polar disc seems to be a result of the direction of gas infall from the filament. We have shown that there is not a single moment when the polar disc 'forms' but, instead, there is a constant evolution of the angular momentum of the infalling gas and stars.

The angular momentum of the last major merger is almost exactly orthogonal to the filament and we feel that this is the most likely origin of the polar disc structure. In this scenario, put forward by Brook et al. (2008), the major merger reorientates the angular momentum of the old stars and the cold gas already present in the disc. Gas continues to flow in from the large-scale structure unaffected by this merger and so builds up the polar disc.

We see that the major merger affects the stars most strongly without any significant influence on the dark halo, and the cold gas recovers its old angular momentum within a Gyr. However, this is not the whole story as subsequent to the major merger there is further evolution in the orientation of the entire galaxy system, potentially due to tumbling or torques from the halo. The growing alignment of the polar disc with the intermediate axis of the dark halo does not seem affected by the major merger.

We also provide a basic comparison of the polar disc galaxy to a classical disc galaxy to better isolate the origin of the extreme behaviour of the polar disc. We also confirm that the polar disc exhibits the characteristics of a disc built up from the inside out, both from the metallicity gradient and the stellar age profile. Clearly, though, any conclusions for their formation, when based upon a single simulated system, must be taken as tentative, at best. We need to (and will) repeat this analysis on a statistically significant sample of simulated polar disc systems.

ACKNOWLEDGMENTS

We wish to thank Greg Stinson for supplying the data on the standard, non-polar, galaxy we used in this paper. ONS acknowledges the support of STFC through its PhD Studentship programme (PPA/S/S/2006/4526) and a fellowship from the European Commissions Framework Programme 7, through the Marie Curie Initial Training Network CosmoComp (PITN-GA-2009-238356). BKG, CBB, RJT and AK acknowledge the support of the UK's Science & Technology Facilities Council (ST/F002432/1, ST/G003025/1). BKG acknowledges the generous visitor support provided by Saint Mary's University and Monash University. AK further acknowledges support by the Spanish Ministerio de Ciencia e Innovacion (MICINN) in Spain through the Ramon y Cajal programme as well as the grants AYA 2009-13875-C03-02, AYA2009-12792-C03-03, CSD2009-00064 and CAM S2009/ESP-1496. This work was made possible by the University of Central Lancashire's High Performance Computing Facility, the San Diego Supercomputing Facility and the UK's National Cosmology Supercomputer (COSMOS). We thank the DEISA consortium, co-funded through EU FP6 project RI-031513 and the FP7 project RI-222919, for support within the DEISA Extreme Computing Initiative. We also thank the referee for their recommendations which greatly improved the paper.

REFERENCES

Abadi M. G., Navarro J. F., Steinmetz M., Eke V. R., 2003, ApJ, 591, 499
Allgood B., Flores R. A., Primack J. R., Kravtsov A. V., Wechsler R. H., Faltenbacher A., Bullock J. S., 2006, MNRAS, 367, 1781
Arnaboldi M., Oosterloo T., Combes F., Freeman K. C., Koribalski B., 1997, AJ, 113, 585
Bailin J., Steinmetz M., 2005, ApJ, 627, 647
Bailin J. et al., 2005, ApJ, 627, L17
Barnes J., Hut P., 1986, Nat, 324, 446
Begeman K. G., Broeils A. H., Sanders R. H., 1991, MNRAS, 249, 523
Bekki K., 1997, ApJ, 490, L37
Bekki K., 1998, ApJ, 499, 635
Boissier S., Prantzos N., 1999, MNRAS, 307, 857
Bournaud F., Combes F., 2003, A&A, 401, 817
Brook C. B., Governato F., Quinn T., Wadsley J., Brooks A. M., Willman B., Stilp A., Jonsson P., 2008, ApJ, 689, 678
Casertano S., van Gorkom J. H., 1991, AJ, 101, 1231
Combes F., Arnaboldi M., 1996, A&A, 305, 763
Combes F., García-Burillo S., Braine J., Schinnerer E., Walter F., Colina L., Gerin M., 2006, A&A, 460, L49
Cox A. L., Sparke L. S., van Moorsel G., 2006, AJ, 131, 828
Gallagher J. S., Sparke L. S., Matthews L. D., Frattare L. M., English J., Kinney A. L., Iodice E., Arnaboldi M., 2002, ApJ, 568, 199
Gill S. P. D., Knebe A., Gibson B. K., 2004, MNRAS, 351, 399
Haardt F., Madau P., 1996, ApJ, 461, 20
Hoekstra H., Yee H. K. C., Gladders M. D., 2004, ApJ, 606, 67
Huchtmeier W. K., 1997, A&A, 319, 401
Iodice E., Arnaboldi M., De Lucia G., Gallagher J. S., III, Sparke L. S., Freeman K. C., 2002, AJ, 123, 195
Iodice E., Arnaboldi M., Bournaud F., Combes F., Sparke L. S., van Driel W., Capaccioli M., 2003, ApJ, 585, 730
Iodice E. et al., 2006, ApJ, 643, 200
Kazantzidis S., Kravtsov A. V., Zentner A. R., Allgood B., Nagai D., Moore B., 2004, ApJ, 611, L73
Knebe A., Libeskind N. I., Knollmann S. R., Yepes G., Gottlöber S., Hoffman Y., 2010, MNRAS, 405, 1119
Knollmann S. R., Knebe A., 2009, ApJS, 182, 608
Kroupa P., 2001, MNRAS, 322, 231
Macciò A. V., Moore B., Stadel J., 2006, ApJ, 636, L25
McGaugh S. S., 2005, ApJ, 632, 859
Matteucci F., Francois P., 1989, MNRAS, 239, 885
Matteucci F., Franco J., Francois P., Treyer M.-A., 1989, Rev. Mex. Astron. Astrofis., 18, 145
Pilkington K. et al., 2012, A&A, 540, 56
Pizagno J. et al., 2005, ApJ, 633, 844
Reshetnikov V., Sotnikova N., 1997, A&A, 325, 933
Roškar R., Debattista V. P., Brooks A. M., Quinn T. R., Brook C. B., Governato F., Dalcanton J. J., Wadsley J., 2010, MNRAS, 408, 783
Rubin V. C., 1994, AJ, 108, 456
Sackett P. D., 1999, in Merritt D. R., Valluri M., Sellwood J. A., eds, ASP Conf. Ser. Vol. 182, Galaxy Dynamics. Astron. Soc. Pac., San Francisco, p. 393
Sackett P. D., Rix H., Jarvis B. J., Freeman K. C., 1994, ApJ, 436, 629
Sánchez-Blázquez P., Courty S., Gibson B. K., Brook C. B., 2009, MNRAS, 398, 591
Schweizer F., Whitmore B. C., Rubin V. C., 1983, AJ, 88, 909
Seljak U., Zaldarriaga M., 1996, ApJ, 469, 437
Sparke L. S., Cox A. L., 2000, in Combes F., Mamon G. A., Charmandaris V., eds, ASP Conf. Ser. Vol. 197, Dynamics of Galaxies: From the Early Universe to the Present. Astron. Soc. Pac., San Francisco, p. 119
Spavone M., Iodice E., Arnaboldi M., Gerhard O., Saglia R., Longo G., 2010, ApJ, 714, 1081
Spavone M., Iodice E., Arnaboldi M., Longo G., Gerhard O., 2011, A&A, 531, A21
Springel V., White S. D. M., Hernquist L., 2004, in Ryder S., Pisano D., Walker M., Freeman K., eds, Proc. IAU Symp. 220, Dark Matter in Galaxies. Astron. Soc. Pac., San Francisco, p. 421
Stinson G., Seth A., Katz N., Wadsley J., Governato F., Quinn T., 2006, MNRAS, 373, 1074
Stinson G. S., Bailin J., Couchman H., Wadsley J., Shen S., Nickerson S., Brook C., Quinn T., 2010, MNRAS, 408, 812
Swaters R. A., Rubin V. C., 2003, ApJ, 587, L23

Tremaine S., Yu Q., 2000, MNRAS, 319, 1
Wadsley J. W., Stadel J., Quinn T., 2004, New Astron., 9, 137
Wechsler R. H., Bullock J. S., Primack J. R., Kravtsov A. V., Dekel A., 2002, ApJ, 568, 52
Whitmore B. C., Lucas R. A., McElroy D. B., Steiman-Cameron T. Y., Sackett P. D., Olling R. P., 1990, AJ, 100, 1489
Williams M. J., Bureau M., Cappellari M., 2010, MNRAS, 409, 1330
Zaldarriaga M., Seljak U., Bertschinger E., 1998, ApJ, 494, 491

This paper has been typeset from a TEX/LATEX file prepared by the author.